Electronic Research Archive

https://www.aimspress.com/journal/era

ERA, 34(1): 351–375.
DOI: 10.3934/era.2026017
Received: 04 November 2025
Revised: 16 December 2025
Accepted: 04 January 2026
Published: 13 January 2026

Research article

Modelling the effects of delayed mortality and saturated incidence on the population dynamics of infected ash trees

Zhenjie Zhang, Yueyang Ding, Nan Jiang*and Ruizhi Yang

Department of Mathematics, Northeast Forestry University, Harbin 150040, China

* **Correspondence:** Email: jngrace@nefu.edu.cn.

Abstract: This study centers on infectious disease models that feature a delayed mortality rate and the Holling II type functional response function. Through a theoretical analysis, it is confirmed that the solutions of the model possess positivity and boundedness, and the equilibrium points are obtained with their local and global stability conditions ascertained. The research indicates that, in the absence of time delay, transcritical and Hopf bifurcations emerge in the model under specific parameter conditions, thus furnishing a foundation to understand the dynamics of disease transmission. Subsequently, a time delay is incorporated into the system, and its impact on the Hopf bifurcation is analyzed. Numerical simulations depict the dynamic behaviors of the model at different delay times. For instance, the system can swiftly reach a stable state without delay, and periodic oscillations occur when the delay surpasses the critical value, thus validating the theory and suggesting that the delayed death factor has a significant influence. By comparing with actual data, the model effectively depicts the spread and lethality of the disease in infected ash trees across different regions, and uncovers the population differences and dynamic change patterns. Thus, it offers targeted strategies for disease prevention and control, as well as the ecological management of ash trees, which is relevant to the study on the impacts of delayed mortality and the Holling-II functional response function on the population dynamics of infected ash trees.

Keywords: bifurcation; delayed mortality; Holling type II; stability

1. Introduction

In recent decades, the world's forested regions have witnessed a sharp and concerning increase in emerging infectious diseases (EIDs), which are intricately linked to invasive forest pathogens (IFPs) that are mainly introduced through human-mediated activities such as international trade and travel. These pathogens have the ability to rapidly spread, thus wreaking havoc on forest ecosystems and resulting in severe mortality events in numerous instances.

Modeling the future losses of forests due to EIDs is an essential forecasting tool for effective management strategies. However, developing an appropriate and accurate model is a challenging task because of the complex interactions that occur within the environment-host-pathogen disease triangle. The European ash tree has been severely impacted by ash dieback, which is caused by the invasive fungus *Hymenoscyphus fraxineus*. The extent of the population decline of the European ash tree and its overall impact remain uncertain [1]. To better study EIDs in the world's forested regions, we first review the recent research progress made by researchers that used mathematical models.

Recently, mathematical models have been widely applied to predict complex relationships in biological populations, such as predation relationships, and a series of new research findings have emerged [2–5]. Meanwhile, infectious disease models in biological populations have gradually developed into an important research direction. In the early 20th century, researchers proposed an infectious disease model based on a large amount of data and facts to describe the transmission process of infectious diseases in a population. They divided the population into two categories: susceptible individuals (S) and infected individuals (I). In recent years, numerous scholars have conducted research on the SI epidemic model and other epidemic models. The majority of them have shown particular interest in the formulation of the incidence rate, specifically the rate at which susceptible individuals become infected through contact with infective ones. Sessile organisms achieve effective pathogen transmission through their interactions [6]. Therefore, in this paper, we propose to establish a model of organism interactions to investigate the infectious disease dynamics of ash tree populations. For instance, in [7], the investigators proposed a classical infectious disease model that employed a bilinear incidence rate as follows:

$$\begin{cases} \dfrac{dS(t)}{dt} = -aS(t)I(t), \\ \dfrac{dI(t)}{dt} = aS(t)I(t) - bI(t), \end{cases} \tag{1.1}$$

where a is the transmission rate, and b represents the rate at which the infected individuals recover. Considering the growth and death of the population, Chen et al. proposed the following model in [8]:

$$\begin{cases} \dfrac{dS(t)}{dt} = S(t)\left(r - eS(t) - aI(t)\right), \\ \dfrac{dI(t)}{dt} = I(t)\left(aS(t) - c - fI(t)\right), \end{cases} \tag{1.2}$$

where the parameters r, a, c, e, and f are positive constants, r is the recruitment rate of the susceptible population, and c is the death rate of the infectives. They defined a threshold and, in combination with this threshold, provided the condition for the global asymptotic stability of the disease-free equilibrium. Taking the carrying capacity of the environment for the population into account, in [9], Wang et al. incorporated logistic growth into the model and obtained the following equation:

$$\begin{cases} \dfrac{dS(t)}{dt} = rS(t)\left(1 - \dfrac{S(t)}{K}\right) - aS(t)I(t) + bI(t), \\ \dfrac{dI(t)}{dt} = aS(t)I(t) - (c + d + b)I, \end{cases} \tag{1.3}$$

where K is the carrying capacity of the community in the absence of infection, and d is the disease-induced death rate.

However, by studying the dynamics of host-parasite, May and Anderson [10] discovered that the quantity of effective contacts between infected and susceptible individuals did not invariably exhibit a linear increase when the incidence rate reached saturation with respect to the susceptibles. Therefore, they introduced the saturated incidence rate $\frac{\beta S(t)}{1+hS(t)}$ to supplement the deficiency of the linear contact rate, where h is the saturated incidence rate [11,12]. This term fully takes the form of incidence function into account, in which the infection rate cannot indefinitely increase due to various that limiting factors in the process of infection, and it is usually used to more realistically simulate the spread of infectious diseases in the population. Mathematically speaking, we have $\frac{\beta S(t)}{1+hS(t)} \to \frac{\beta}{h}$ as $S(t) \to \infty$. Similar to the predator-prey model, customarily, we refer to the term with the saturated incidence rate as the Holling type functional response function. Additionally, we refer to the term in the form of $\beta S(t)$ as Holling type I and the term in the form of $\frac{\beta S(t)}{1+hS(t)}$ as Holling type II. If $h = 0$, then the model will become linear, that is, of the Holling-I type. When the density of ash trees is high, the efficiency of infectious disease transmission does not indefinitely increase. Thus, we adopt the Holling Type II functional response function to accurately simulate this transmission ceiling.

Motivated by the above work, we will study the following system with the Holling type II functional response:

$$\begin{cases} \dfrac{dS(t)}{dt} = rS(t)\left(1 - \dfrac{S(t) + I(t)}{K}\right) - \dfrac{\beta S(t)I(t)}{1 + hS(t)} - \mu S(t), \\ \dfrac{dI(t)}{dt} = \dfrac{\beta S(t)I(t)}{1 + hS(t)} - \mu I(t) - \rho I(t - \tau), \end{cases} \tag{1.4}$$

where r is the intrinsic growth rate, K stands for the environmental carrying capacity, β is the transmission rate, μ represents the natural mortality rate of the two populations, ρ is the delayed mortality rate, and τ is the time delay of the death of infected saplings, which means that the infected ash saplings will die after τ years. To make the model biologically meaningful, we assume that r, K, β, μ, h, ρ, and τ are all positive constants. Meanwhile, we also assume that $r > \mu$, that is, the growth rate is greater than the natural mortality rate.

To clarify the development of infectious diseases in ash tree populations, this study intends to establish a dedicated prediction model. By adopting the Holling-Type II functional response function, the impact of the delayed mortality rate of infected populations on the progression of infectious diseases is investigated. By analyzing equilibrium points and various bifurcation properties, the study aims to reveal the transmission trends of the diseases. Meanwhile, a sensitivity analysis is employed to clarify the influence of the model's parameters on the transmission process, thus providing theoretical support for relevant prevention, control, and management efforts.

The rest of this paper is organized as follows: in Section 2, we study the positivity and boundedness of the solution; in Section 3, we study the stability of equilibrium points and the existence of bifurcations, and we discuss the global stability of the equilibrium points; in Section 4, we study the property of the Hopf bifurcation; in Section 5, we give some numerical simulations to illustrate the theoretical results; in Section 6, we conduct a sensitivity analysis; and in Section 7, we give a short conclusion.

2. Positivity and boundedness of the solution

In this section, we discuss the positivity and boundedness of the solution of the system without a time delay. If $\tau = 0$, then system (1.4) becomes the following:

$$\begin{cases} \dfrac{dS}{dt} = rS\left(1 - \dfrac{S+I}{K}\right) - \dfrac{\beta S I}{1+hS} - \mu S, \\ \dfrac{dI}{dt} = \dfrac{\beta S I}{1+hS} - \mu I - \rho I. \end{cases} \tag{2.1}$$

Let $\Omega_0 = \{(S, I)|S > 0, I > 0\}$. For practical biological meaning, we simply study system (1.4) in $\overline{\Omega_0}$.

Lemma 2.1. *From the first equation of system* (2.1)*,*

$$\lim_{t\to\infty} S(t) \leq \frac{K(r-\mu)}{r} \triangleq \overline{S}. \tag{2.2}$$

Proof. Based on the first equation of system (2.1),it follows that $\frac{dS}{dt} = S\left(r\left(1 - \frac{S+I}{K}\right) - \frac{\beta I}{1+hS} - \mu\right)$; then, $\frac{dS}{dt} \leq S\left(r - \mu - \frac{rS}{K}\right)$. By applying the standard comparison lemma [13] , the aforementioned inequality signifies that $\lim_{t\to\infty} S(t) \leq \overline{S}$, where $\overline{S}$ is a positive real root of equation $r - \mu - \frac{rS}{K} = 0$. By solving the above equation, we obtain $\overline{S} = \frac{K(r-\mu)}{r}$.

The proof is complete. □

Lemma 2.2. *The solution* $(S(t), I(t))$ *of system* (2.1) *with initial values* $S(0) \geq 0, I(0) \geq 0$ *are positive and bounded for all* $t \geq 0$.

Proof. Since model (1.4) is of Kolmogorov type [14], the solution $(S(t), I(t))$ with initial values $S(0) \geq 0, I(0) \geq 0$ are positive for all $t \geq 0$. Therefore, we only give a bounded proof of the solution. By (2.2), given any $\varepsilon > 0, S(t) \leq \overline{S} + \varepsilon$ for a sufficiently large t. Define the function $N = S + I$; differentiating with respect to N gives the following:

$$\frac{dN}{dt} = \frac{dS}{dt} + \frac{dI}{dt} = rS\left(1 - \frac{S+I}{K}\right) - \mu(S+I) - \rho I \leq rS\left(1 - \frac{S+I}{K}\right) - \mu N.$$

Since S is bounded, as established in Lemma 2.1, the quadratic term attains its maximum at $\frac{K}{2}$. Therefore, $\frac{dN}{dt} \leq \frac{rK}{4} - \mu N$, from which the boundedness of N follows, and subsequently also that of I, which completes the proof. □

3. Stability analysis of the model without time delay

Mathematically speaking, the equilibrium points of an equation set are the values that meet the requirements of the model system in its stationary states.

3.1. The existence and stability of the equilibrium points of the model system

Lemma 3.1. *The model system* (2.1) *has two boundary equilibrium points:* $E_0(0, 0)$ *and* $E_1(\frac{K(r-\mu)}{r}, 0)$. *Additionally, if* $(\mathbf{H_1})$ *and* $(\mathbf{H_2})$ *hold, then the model system has a unique positive equilibrium* $E^*(S^*, I^*)$.

Proof. Hence, the equilibrium points of the model system (2.1) can be acquired by resolving the following two equations:

$$\begin{cases} rS\left(1-\dfrac{S+I}{K}\right)-\dfrac{\beta SI}{1+hS}-\mu S=0, \\ \dfrac{\beta SI}{1+hS}-\mu I-\rho I=0. \end{cases} \tag{3.1}$$

By solving the first equation of (3.1), we find $S = 0, I = \frac{(K(r-\mu)-rS)(1+hS)}{r(1+hS)-\beta K}$. By solving the second equation of (3.1), we can obtain $I = 0$ and $S = \frac{\mu+\rho}{\beta-h(\mu+\rho)}$. Substituting $I = 0$ in the first equation of (3.1), we can obtain $S = \frac{K(r-\mu)}{r}$. Hence, the system model (2.1) has two boundary equilibria: $E_0(0, 0)$ and $E_1(\frac{K(r-\mu)}{r}, 0)$. Additionally, if the model system has a positive equilibrium $E^*(S^*, I^*)$,where $S^* = \frac{\mu+\rho}{\beta-h(\mu+\rho)}$, $I^* = \frac{(K(r-\mu)-rS^*)(1+hS^*)}{r(1+hS^*)-\beta K}$, then we need to make $\beta - h(\mu + \rho) > 0$ satisfied. Then, we substitute S^* into I^* and simplify it by using the fact that $I^* > 0$. After a series of simplifications, we can make the above conditions equivalent to

$$(\mathbf{H_1}) \quad \beta - h(\mu + \rho) > 0,$$

and

$$(\mathbf{H_2}) \quad \mu - r + \frac{r(\mu + \rho)}{K(\beta - h(\mu + \rho))} < 0.$$

The proof is complete. □

Theorem 3.1. *(i) The equilibrium point E_0 always exists and is a saddle point.*
(ii) The equilibrium point E_1 always exists and is a locally asymptotically stable if $(\mathbf{H_3})$ *holds.*

Proof. (i) Through simple calculations, the Jacobian matrix of the model system (2.1) at E_0 is given by the following:

$$J_{E_0} = \begin{pmatrix} r-\mu & 0 \\ 0 & -(\mu+\rho) \end{pmatrix}.$$

Obviously, it has two eigenvalues: $\lambda_1 = r - \mu$ and $\lambda_2 = -(\mu + \rho)$. According to the assumption, we can get that $\lambda_1 > 0$,$\lambda_2 < 0$. Thus, E_0 is a saddle point.
(ii) The Jacobian matrix of the model system (2.1) at E_1 is given by the following:

$$J_{E_1} = \begin{pmatrix} \mu - r & A_1 \\ 0 & A_2 \end{pmatrix},$$

where $A_1 = \frac{(\mu-r)(r+rhK+K(\beta-h\mu))}{r+rhK-hK\mu}$, and $A_2 = \frac{\beta K(r-\mu)}{r+hK(r-\mu)} - \mu - \rho$. Obviously, it has two eigenvalues: $\lambda_3 = \mu - r$ and $\lambda_4 = A_2$. According to the assumption, we can get that $\lambda_3 < 0$. Additionally, if the basic reproductive number

$$(\mathbf{H_3}) \quad \mathcal{R}_0 = \frac{\beta K(r-\mu)}{(r + hK(r-\mu))(\mu+\rho)} < 1,$$

then we can easily obtain $\lambda_4 < 0$. Then, we obtain that E_1 is locally asymptotically stable if $(\mathbf{H_3})$ holds.
The proof is complete. □

Theorem 3.2. *The equilibrium point E^* is locally stable if* $(\mathbf{H_4})$ *holds.*

Proof. Through simple calculations, the Jacobian matrix of the model system (2.1) at E^* is given by the following:

$$J_{E^*} = \begin{pmatrix} r-\mu-\frac{r(2S^*+I^*)}{K}-\frac{\beta I^*}{(1+hS^*)^2} & -\frac{S^*(r+rhS^*+\beta K)}{K(1+hS^*)} \\ \frac{\beta I^*}{(1+hS^*)^2} & 0 \end{pmatrix}.$$

Obviously, $det(J_{E^*}) > 0$. According to Routh-Hurwitz criterion [15], if $tr(J_{E^*}) < 0$ holds, then the equilibrium point E^* is locally stable, where $det(J_{E^*})$ represents the determinant of matrix J_{E^*}, and $tr(J_{E^*})$ represents the trace of matrix J_{E^*}. Furthermore, if

$$(\mathbf{H_4}) \quad r-\mu-\frac{r(2S^*+I^*)}{K}-\frac{\beta I^*}{(1+hS^*)^2} < 0$$

holds, then the equilibrium point E^* is locally stable.

The proof is complete. □

3.2. Global stability of the equilibrium points

In this section, we discuss the global asymptotically stability (GAS) of the boundary equilibrium $E_1(\frac{K(r-\mu)}{r}, 0)$ and the positive equilibrium $E^*(S^*, I^*)$.

Theorem 3.3. *The boundary equilibrium point $E_1(\frac{K(r-\mu)}{r}, 0)$ is GAS if $(\mathbf{H_3})$ holds.*

Proof. From the second equation of (2.1), we can obtain the following:

$$\frac{dI}{dt} \le \frac{\beta K(r-\mu)}{r+hK(r-\mu)} I - (\rho+\mu)I.$$

By the comparison principle

$$\limsup_{t\to\infty} I(t) \le I(0)\exp\left[\frac{\beta K(r-\mu)}{r+hK(r-\mu)} - (\rho+\mu)\right]t,$$

if $(\mathbf{H_3})$ holds, we can obtain that $\limsup_{t\to\infty} I(t) = 0$. Therefore, for any $\epsilon > 0$, there exists a $T > 0$ such that when $t > T$, $I(t) < \epsilon$ holds. Substituting it into the first equation of (2.1), we have the following:

$$\frac{dS}{dt} \ge rS\left(1-\frac{S+\epsilon}{K}\right) - \frac{\beta S\epsilon}{1+hS} - \mu S = \left[r\left(1-\frac{S+\epsilon}{K}\right) - \frac{\beta\epsilon}{1+hS} - \mu\right]S.$$

Thus, $\lim_{t\to\infty} S(t) = \frac{K(r-\mu)}{r}$. Therefore, we have proved that the equilibrium point $E_1(\frac{K(r-\mu)}{r}, 0)$ is GAS if $(\mathbf{H_3})$ holds. The proof is complete. □

Theorem 3.4. *If $\frac{r}{K} \ge \frac{\beta h I^*}{1+hS^*}$ holds, then the positive equilibrium point $E^*(S^*, I^*)$ is GAS.*

Proof. The Lyapunov function is defined as follows:

$$V = \left(S - S^* - S^*\ln\frac{S}{S^*}\right) + \nu\left(I - I^* - I^*\ln\frac{I}{I^*}\right). \tag{3.2}$$

The time derivative of V is given as follows along with the solution of (2.1):

$$\begin{aligned}\frac{dV}{dt} &= \frac{S-S^*}{S}\frac{dS}{dt} + \nu\frac{I-I^*}{I}\frac{dI}{dt}\\ &= \frac{S-S^*}{S}\left(rS\left(1-\frac{S+I}{K}\right)-\frac{\beta SI}{1+hS}-\mu S\right)+\nu\frac{I-I^*}{I}\left(\frac{\beta SI}{1+hS}-\mu I-\rho I\right)\\ &= (S-S^*)\left(r\left(1-\frac{S+I}{K}\right)-\frac{\beta I}{1+hS}-\mu\right)+\nu(I-I^*)\left(\frac{\beta S}{1+hS}-\mu-\rho\right)\\ &= (S-S^*)\left(r\frac{S^*+I^*}{K}+\frac{\beta I^*}{1+hS^*}-r\frac{S+I}{K}-\frac{\beta I}{1+hS}\right)+\nu(I-I^*)\left(\frac{\beta S}{1+hS}-\frac{\beta S^*}{1+hS^*}\right)\\ &= (S-S^*)^2\left(-\frac{r}{K}+\frac{\beta hI^*}{(1+hS)(1+hS^*)}\right)+(S-S^*)(I-I^*)\left(-\frac{r}{K}+\frac{\beta(\nu-1-hS^*)}{(1+hS)(1+hS^*)}\right).\end{aligned}$$

According to Lemma 2.1, we can obtain $\lim_{t\to\infty} S(t) \le \overline{S}$. Then, we obtain the following:

$$\frac{dV}{dt} \le (S-S^*)^2\left(-\frac{r}{K}+\frac{\beta hI^*}{1+hS^*}\right)+(S-S^*)(I-I^*)\left(-\frac{r}{K}+\frac{\beta(\nu-1-hS^*)}{(1+h\overline{S})(1+hS^*)}\right).$$

Choosing ν such that $\frac{r}{K} = \frac{\beta(\nu-1-hS^*)}{(1+h\overline{S})(1+hS^*)}$, we obtain the following:

$$\frac{dV}{dt} \le (S-S^*)^2\left(-\frac{r}{K}+\frac{\beta hI^*}{1+hS^*}\right). \tag{3.3}$$

Thus, $\frac{dV}{dt} < 0$ if $\frac{r}{K} \ge \frac{\beta hI^*}{1+hS^*}$ holds, which ensures the GAS of equilibrium point $E^*(S^*, I^*)$.

The proof is complete. □

3.3. Analysis of bifurcations

Within this section, the presence of several types of bifurcations, namely the transcritical bifurcation and the Hopf bifurcation, is examined for particular system parameter values that concern the axial and equilibrium points.

3.3.1. Transcritial bifurcation

In this subsection, we discuss the existence of a transcritical bifurcation in the model system (2.1) about the boundary equilibrium point $E_1(\frac{K(r-\mu)}{r}, 0)$.

Theorem 3.5. *The model system* (2.1) *experiences a transcritical bifurcation with respect to the equilibrium point E_1 when the system parameter ρ reaches the critical value of $\rho = \rho^{[TC]}$, where $\rho^{[TC]} = \frac{\beta K(r-\mu)}{r+hK(r-\mu)} - \mu$.*

Proof. Regarding the crucial system parameter value $\rho^{[TC]} = \frac{\beta K(r-\mu)}{r+hK(r-\mu)} - \mu$, the Jacobian matrix J_{E_1} may be represented as follows:

$$J_{E_1} = \begin{pmatrix} \mu - r & A_1 \\ 0 & 0 \end{pmatrix}.$$

Thus, the Jacobian matrix possesses a single zero eigenvalue. At this moment, assume that V and W are the eigenvectors that correspond to the simple zero eigenvalue of the Jacobian matrix J_{E_1} and its

transpose, respectively. Subsequently, regarding the value of the system parameter $\rho^{[TC]} = \frac{\beta K(r-\mu)}{r+hK(r-\mu)} - \mu$ at the threshold, the eigenvectors are given by $V = (r-\mu, -\frac{(r-\mu)[r+rhK+K(\beta-h\mu)]}{r+hK(r-\mu)})^T = (v_1, v_2)^T$ and $W = (0,1)^T = (w_1, w_2)^T$. The transversality conditions are given by the following:

$$\begin{aligned}
&W^T f_\rho(E_1; \rho = \rho^{[TC]}) = 0,\\
&W^T [Df_\rho(E_1; \rho = \rho^{[TC]})V] = \frac{(r-\mu)[r+rhK+K(\beta-h\mu)]}{r+hK(r-\mu)} \neq 0,\\
&W^T [D^2 f(E_1; \rho = \rho^{[TC]})(V,V)] = \frac{2\beta r^2 v_1 v_2}{[r+hK(r-\mu)]^2} \neq 0.
\end{aligned}$$

As a result, in accordance with Sotomayor's theorem [16], the calculated transversality conditions presented above indicate that a transcritical bifurcation takes place in the model system (2.1) near the equilibrium point E_1 at the moment when $\rho = \rho^{[TC]}$.

The proof is complete. □

3.3.2. Stability analysis of the Hopf bifurcation

In the current subsection, the emergence of a Hopf bifurcation within the model system (2.1) in relation to the positive equilibrium E^* is examined, and its stability characteristics are analyzed through the computation of the first Lyapunov number $\mathcal{L}_1$.

The Jacobian matrix of the model system (2.1) at any arbitrary point (S, I) is given by the following:

$$J(S,I) = \begin{pmatrix} r-\mu-\frac{r(2S+I)}{K} - \frac{\beta I}{(1+hS)^2} & -\frac{S(r+rhS+\beta K)}{K(1+hS)} \\ \frac{\beta I}{(1+hS)^2} & \frac{\beta S}{1+hS} - \mu - \rho \end{pmatrix} = (J_{ij})_{2\times 2}; i, j = 1, 2.$$

Additionally, the characteristic equation of the Jacobian matrix can be expressed as follows:

$$\lambda^2 - T\lambda + D = 0, \tag{3.4}$$

where $T = J_{11} + J_{22}$, and $D = J_{11}J_{22} - J_{12}J_{21}$.

Theorem 3.6. *When the system parameter h attains the value $h = h^{[HB]}$, the model system* (2.1) *will have a Hopf bifurcation and produce a limit cycle that encloses the equilibrium point E^*, given that three conditions are satisfied: $T(h^{[HB]}) = 0$, $D(h^{[HB]}) > 0$, and $\dot{T}(h^{[HB]}) \neq 0$.*

Proof. As the system parameter h reaches the critical value $h = h^{[HB]}$, the characteristic equation (3.4) can be formulated as $\lambda^2 + D(h) = 0$. At this moment, the characteristic equation harbors a pair of purely imaginary eigenvalues, precisely $\lambda_{1,2} = \pm i\sqrt{D(h)}$. Furthermore, because T and D are smooth functions with regard to h, the eigenvalues of the Jacobian matrix J_{E_*} have the form $\lambda_{1,2} = \sigma_1(h) \pm \sigma_2(h)$. Here, $\sigma_1(h)$ and $\sigma_2(h)$ are defined within an open interval that includes the critical value $h^{[HB]}$, and both are continuous functions of h.

Now, to check the Hopf bifurcation in the model system (2.1), we will try to work out the transversality condition as follows:

$$\frac{d}{dh}(\mathrm{Re}\lambda_i(h))|_{h=h^{[HB]}} \neq 0; i = 1, 2.$$

Put $\lambda_{1,2} = \sigma_1(h) + \sigma_2(h)$ in the characteristic equation and differentiate on each side regarding h; thus, we obtain $2(\dot{\sigma_1} + \dot{\sigma_2})(\sigma_1 + \sigma_2) - T(\dot{\sigma_1} + \dot{\sigma_2}) - \dot{T}(\sigma_1 + \sigma_2) + \dot{D} = 0$. Furthermore, we can get that

$$\begin{cases} a_1\dot{\sigma_1} - a_2\dot{\sigma_2} = b_1, \\ a_2\dot{\sigma_1} + a_1\dot{\sigma_2} = b_2, \end{cases} \tag{3.5}$$

where $a_1 = 2\sigma_1 - T, a_2 = 2\sigma_2, b_1 = \dot{T}\sigma_1 - \dot{D}, b_2 = \dot{T}\sigma_2$. By Cramer's Rule, we can obtain $\dot{\sigma_1} = \frac{a_1b_1+a_2b_2}{a_1^2+a_2^2}$. Thus, in the case of the critical system parameter value $h = h^{[HB]}$, the following scenarios could be considered:

Case-I: For $\sigma_1 = 0, \sigma_2 = \sqrt{D}$. We have $a_1 = 0, a_2 = 2\sqrt{D}, b_1 = \dot{D}, b_2 = \dot{T}\sqrt{D}$. Thus, one may have $\dot{\sigma_1}|_{h=h^{[HB]}} = \frac{2\dot{T}D}{4D}|_{h=h^{[HB]}} = \frac{1}{2}\dot{T}|_{h=h^{[HB]}} = \frac{1}{2}\frac{dT}{dh}|_{h=h^{[HB]}} \neq 0$.

Case-II: For $\sigma_1 = 0, \sigma_2 = -\sqrt{D}$. We have $a_1 = 0, a_2 = -2\sqrt{D}, b_1 = \dot{D}, b_2 = -\dot{T}\sqrt{D}$. So, one may have $\dot{\sigma_1}|_{h=h^{[HB]}} = \frac{2\dot{T}D}{4D}|_{h=h^{[HB]}} = \frac{1}{2}\dot{T}|_{h=h^{[HB]}} = \frac{1}{2}\frac{dT}{dh}|_{h=h^{[HB]}} \neq 0$.

The proof is complete. □

Subsequently, we proceed to analyze the direction and stability of the Hopf bifurcation. Initially, we shift the equilibrium point E^* to the origin through the transformation $X_1 = S - S^*, X_2 = I - I^*$. Consequently, the model system (2.1) is converted into the following form:

$$\begin{cases} \dfrac{dX_1}{dt} = r(X_1 + S^*)\left(1 - \dfrac{(X_1 + S^*) + (X_2 + I^*)}{K}\right) - \dfrac{\beta(X_1 + S^*)(X_2 + I^*)}{1 + h(X_1 + S^*)} - \mu(X_1 + S^*), \\ \dfrac{dX_2}{dt} = \dfrac{\beta(X_1 + S^*)(X_2 + I^*)}{1 + h(X_1 + S^*)} - (\mu + \rho)(X_2 + I^*). \end{cases} \tag{3.6}$$

By conducting a Taylor series expansion centered at the origin, one can derive the following:

$$\begin{aligned} \dot{X}_1 &= a_{10}X_1 + a_{01}X_2 + a_{20}X_1^2 + a_{11}X_1X_2 + a_{02}X_2^2 + a_{30}X_1^3 + a_{21}X_1^2X_2 + a_{12}X_1X_2^2 + a_{03}X_2^3 + o(\|X\|^4), \\ \dot{X}_2 &= b_{10}X_1 + b_{01}X_2 + b_{20}X_1^2 + b_{11}X_1X_2 + b_{02}X_2^2 + b_{30}X_1^3 + b_{21}X_1^2X_2 + b_{12}X_1X_2^2 + b_{03}X_2^3 + o(\|X\|^4), \end{aligned} \tag{3.7}$$

where the coefficients $a_{ij}, b_{ij}; i, j = 0, 1, 2, 3, ...$ are specified as follows:

$$\begin{aligned} a_{10} &= r\left(1 - \frac{2S^* + I^*}{K}\right) + \frac{\beta hS^*I^*}{(1 + hS^*)^2} - \frac{\beta I^*}{1 + hS^*} - \mu, a_{01} = -\frac{rS^*}{K} - \frac{\beta S^*}{1 + hS^*}, \\ a_{20} &= -\frac{r}{K} - \frac{\beta h^2S^*I^*}{(1 + hS^*)^3} + \frac{\beta hI^*}{(1 + hS^*)^2}, a_{11} = -\frac{r}{K} + \frac{\beta hS^*}{(1 + hS^*)^2} - \frac{\beta}{1 + hS^*}, a_{02} = 0, \\ a_{30} &= \frac{\beta h^3S^*I^*}{(1 + hS^*)^4} - \frac{\beta h^2S^*I^*}{(1 + hS^*)^3}, a_{21} = -\frac{\beta h^2S^*}{(1 + hS^*)^3} + \frac{2\beta h}{(1 + hS^*)^2}, a_{12} = 0, a_{03} = 0, \\ b_{10} &= -\frac{\beta hS^*I^*}{(1 + hS^*)^2} + \frac{\beta I^*}{1 + hS^*}, b_{01} = \frac{\beta S^*}{1 + hS^*} - \mu - \rho, b_{20} = \frac{\beta h^2S^*I^*}{(1 + hS^*)^3} - \frac{\beta hI^*}{(1 + hS^*)^2}, \\ b_{11} &= -\frac{\beta hS^*}{(1 + hS^*)^2} + \frac{\beta}{1 + hS^*}, b_{02} = 0, b_{30} = -\frac{\beta h^3S^*I^*}{(1 + hS^*)^4} + \frac{\beta h^2I^*}{(1 + hS^*)^3}, \\ b_{21} &= \frac{\beta h^2S^*}{(1 + hS^*)^3} - \frac{\beta h}{(1 + hS^*)^2}, b_{12} = 0, b_{03} = 0. \end{aligned}$$

Hence, Eq (3.7) can be expressed in the following manner:

$$\dot{X} = J_{E^*}X + A(X), \tag{3.8}$$

where $X = (X_1, X_2)^T$ and

$$A(X) = \begin{pmatrix} a_{20}X_1^2 + a_{11}X_1X_2 + a_{02}X_2^2 + a_{30}X_1^3 + a_{21}X_1^2X_2 + a_{12}X_1X_2^2 + a_{03}X_2^3 \\ b_{20}X_1^2 + b_{11}X_1X_2 + b_{02}X_2^2 + b_{30}X_1^3 + b_{21}X_1^2X_2 + b_{12}X_1X_2^2 + b_{03}X_2^3 \end{pmatrix} = \begin{pmatrix} A_1(X) \\ A_2(X) \end{pmatrix}.$$

Afterward, the eigenvector ϕ related to the eigenvalue $\lambda = i\sqrt{D}$ of the Jacobian matrix J_{E^*} is expressed as $\phi = (a_{01}, i\sqrt{D} - a_{10})^T$. Then, we define $\Phi = (Re\phi, -Im\phi)$. Next, we can take into account the transformation $X = \Phi Y$ or $Y = \Phi^{-1}X$, with $Y = (Y_1, Y_2)^T$ into account. By applying this transformation to the model system (3.8), we can get $\dot{Y} = (\Phi^{-1}J_{E^*}\Phi)Y + \Phi^{-1}A(\Phi Y)$. This can be shown as follows:

$$\begin{bmatrix} \dot{Y}_1 \\ \dot{Y}_2 \end{bmatrix} = \begin{bmatrix} 0 & -\sqrt{D} \\ \sqrt{D} & 0 \end{bmatrix} \begin{bmatrix} Y_1 \\ Y_2 \end{bmatrix} + \begin{bmatrix} D^1(Y_1, Y_2; h = h^{[HB]}) \\ D^2(Y_1, Y_2; h = h^{[HB]}) \end{bmatrix},$$

where the terms D^1 and D^2 are specified as $D^1(Y_1, Y_2; h = h^{[HB]}) = \frac{1}{a_{01}}A_1$ and $D^2(Y_1, Y_2; h = h^{[HB]}) = -\frac{1}{a_{01}\sqrt{D}}(a_{10}A_1 + a_{01}A_2)$, respectively. Consequently, the computational expression for the first Lyapunov number $\mathcal{L}_1$ relevant to the determination of the stability or instability of the bifurcating limit cycle is presented as follows:

$$\mathcal{L}_1 = \frac{1}{16}\left[D^1_{111} + D^1_{122} + D^2_{112} + D^2_{222}\right] + \frac{1}{16\sqrt{D}}\left[D^1_{12}(D^1_{11} + D^1_{22}) - D^2_{12}(D^2_{11} + D^1_{22}) - D^1_{11}D^2_{11} + D^1_{22}D^2_{22}\right],$$

where $D^k_{ij} = \frac{\partial^2 D^k}{\partial Y_i \partial Y_j}|_{(Y_1,Y_2;h)=(0,0;h^{[HB]})}$, and $D^k_{ijl} = \frac{\partial^3 D^k}{\partial Y_i \partial Y_j \partial Y_l}|_{(Y_1,Y_2;h)=(0,0;h^{[HB]})}$.

Therefore, depending upon the sign of $\mathcal{L}_1$, we have the following theorem.

Theorem 3.7. *(i) If $\mathcal{L}_1 > 0$, then the Hopf bifurcation is supercritical and subsequently, and a stable limit cycle emerges in the vicinity of the positive equilibrium point E^*.*
(ii) If $\mathcal{L}_1 < 0$, then the Hopf bifurcation is subcritical and subsequently, and a limit cycle with instability will emerge in the vicinity of the positive equilibrium E^*.

4. Property of Hopf bifurcation with time delay

In this part, we focus on examining the characteristics of the Hopf bifurcation under the condition of $\tau > 0$, including its existence and stability.

4.1. Existence of Hopf bifurcation

Through simple calculations, the Jacobian matrix that corresponds to the model system (1.4) at the equilibrium point E^* is presented as follows:

$$J_{E^*} = \begin{pmatrix} r - \mu - \frac{r(2S^*+I^*)}{K} - \frac{\beta I^*}{(1+hS^*)^2} & -\frac{rS^*}{K} - \frac{\beta}{1+hS^*} \\ \frac{\beta I^*}{(1+hS^*)^2} & \frac{\beta S^*}{1+hS^*} - \mu - \rho e^{-\lambda\tau} \end{pmatrix}. \tag{4.1}$$

The characteristic equation associated with (4.1) is expressed as follows:

$$\lambda^2 - (J_{11} + J_{22})\lambda + \rho e^{-\lambda\tau}(\lambda - J_{11}) + J_{11}J_{22} - J_{12}J_{21} = 0, \tag{4.2}$$

where $J_{11} = r - \mu - \frac{r(2S^*+I^*)}{K} - \frac{\beta I^*}{(1+hS^*)^2}$, $J_{12} = -\frac{rS^*}{K} - \frac{\beta}{1+hS^*}$, $J_{21} = \frac{\beta I^*}{(1+hS^*)^2}$, $J_{22} = \frac{\beta S^*}{1+hS^*} - \mu$. Assume that there exists a positive τ_0 for which Eq (4.2) has a pair of purely imaginary roots $\pm i\omega$ ($\omega > 0$). In this case, ω complies with the following:

$$-\omega^2 - i(J_{11} + J_{22})\omega + \rho(cos(-\omega\tau) + isin(-\omega\tau))(i\omega - J_{11}) + J_{11}J_{22} - J_{12}J_{21} = 0. \tag{4.3}$$

By splitting into the real and imaginary segments, we obtain the following:

$$\begin{aligned} &-\omega^2 - \rho sin(\omega\tau)\omega + \rho cos(\omega\tau)J_{11} + J_{11}J_{22} - J_{12}J_{21} = 0, \\ &(J_{11} + J_{22})\omega + \rho cos(\omega\tau)\omega + \rho sin(\omega\tau)J_{11} = 0, \end{aligned} \tag{4.4}$$

which is equivalent to

$$\omega^4 + B\omega^2 + C = 0, \tag{4.5}$$

where $B = J_{11}^2 + J_{22}^2 + 2J_{12}J_{21} - \rho^2$, and $C = J_{11}^2J_{22}^2 + J_{12}^2J_{21}^2 - 2J_{11}J_{22}J_{12}J_{21} - \rho^2J_{11}^2$. Since $\omega > 0$, in order to make Eq (4.5) have at least one positive root, we first need to ensure that the discriminant $\Delta \geq 0$. Next, we will conduct a classified discussion on the sign of C. In the case of $C < 0$, it is evident that Eq (4.5) possesses a positive root. In the situation where $C \geq 0$, provided that Eq (4.5) has a positive root, the requirement of $B \leq 0$ has to be fulfilled. Set the positive root of this equation as ω_0, and we can get $\omega_0 = \frac{1}{\sqrt{2}}\sqrt{-B + \sqrt{B^2 - 4C}}$.

Additionally, (4.4) is the same as the following equations:

$$\begin{aligned} &-\omega_0^2 - \rho sin(\omega_0\tau)\omega_0 + \rho cos(\omega_0\tau)J_{11} + J_{11}J_{22} - J_{12}J_{21} = 0, \\ &-J_{11}(J_{11} + J_{22}) - \rho cos(\omega_0\tau)J_{11} + \frac{\rho}{\omega_0}sin(\omega_0\tau)J_{11}^2 = 0. \end{aligned} \tag{4.6}$$

By adding the two equations in (4.6), we can obtain $sin(\omega_0\tau) = \frac{\omega_0^3 + J_{11}^2\omega_0 + J_{12}J_{21}\omega_0}{\rho J_{11}^2 + \rho\omega_0^2}$. We can derive that

$$\tau^* = \frac{1}{\omega_0}\left(arcsin\frac{\omega_0^3 + J_{11}^2\omega_0 + J_{12}J_{21}\omega_0}{\rho J_{11}^2 + \rho\omega_0^2} + 2k\pi\right), k = 0, 1, 2, ... \tag{4.7}$$

Then, a positive τ_0 exists so that (4.2) has a pair of purely imaginary roots $\pm i\omega_0$ when $\tau = \tau_0$, and all eigenvalues possess negative real parts for $\tau \in (0, \tau_0)$.

To get the Hopf bifurcation, we must check the transversal condition of the complex eigenvalues of E^* at $\tau = \tau^*$.

Let $\lambda(\tau) = \alpha(\tau) + i\beta(\tau)$ be the root of the characteristic equation (4.2). Then, $\alpha(\tau^*) = 0, \beta(\tau^*) = \omega_0$. By differentiating each side of the characteristic equation (4.2) with regard to τ at the same time, we are able to obtain the following:

$$\begin{aligned} &2\lambda\frac{d\lambda}{d\tau} - (J_{11} + J_{22})\frac{d\lambda}{d\tau} - \rho e^{-\lambda\tau}\left(\lambda + \tau\frac{d\lambda}{d\tau}\right)(\lambda - J_{11}) + \rho e^{-\lambda\tau}\frac{d\lambda}{d\tau} = 0, \\ &2\lambda\frac{d\lambda}{d\tau} - (J_{11} + J_{22})\frac{d\lambda}{d\tau} - \rho e^{-\lambda\tau}\left(\lambda^2 - \lambda J_{11} + \lambda\tau\frac{d\lambda}{d\tau} - \tau J_{11}\frac{d\lambda}{d\tau}\right)(\lambda - J_{11}) + \rho e^{-\lambda\tau}\frac{d\lambda}{d\tau} = 0, \\ &\frac{d\lambda}{d\tau}\left(2\lambda - J_{11} - J_{22} - \lambda\tau\rho e^{-\lambda\tau} + \tau J_{11}\rho e^{-\lambda\tau} + \rho e^{-\lambda\tau}\right) - \rho e^{-\lambda\tau}\left(\lambda^2 - J_{11}\lambda\right) = 0. \end{aligned}$$

After rearranging the above formula, we can obtain the following:

$$\frac{d\lambda}{d\tau} = \frac{\lambda\rho e^{-\lambda\tau}(\lambda - J_{11})}{2\lambda - J_{11} - J_{22} - \lambda\tau\rho e^{-\lambda\tau} + \tau J_{11}\rho e^{-\lambda\tau} + \rho e^{-\lambda\tau}}. \tag{4.8}$$

By simultaneously taking reciprocals of both sides of the above equation, one may have the following:

$$\begin{aligned}\left(\frac{d\lambda}{d\tau}\right)^{-1} &= \frac{2\lambda - J_{11} - J_{22} - \lambda\tau\rho e^{-\lambda\tau} + \tau J_{11}\rho e^{-\lambda\tau} + \rho e^{-\lambda\tau}}{\lambda\rho e^{-\lambda\tau}(\lambda - J_{11})} \\ &= \frac{2\lambda - J_{11} - J_{22}}{\lambda\rho e^{-\lambda\tau}(\lambda - J_{11})} + \frac{1}{\lambda(\lambda - J_{11})} - \frac{\tau}{\lambda}.\end{aligned} \tag{4.9}$$

Moreover, we may obtain the following:

$$\begin{aligned}\mathrm{Re}\left[\left(\frac{d\lambda}{d\tau}\right)^{-1}|_{\tau=\tau^*,\lambda=i\omega_0}\right] &= Re\left[\left(\frac{2\lambda - J_{11} - J_{22}}{\lambda\rho e^{-\lambda\tau}(\lambda - J_{11})} + \frac{1}{\lambda(\lambda - J_{11})}\right)|_{\tau=\tau^*,\lambda=i\omega_0}\right] \\ &= Re\left[\left(\frac{2\lambda - J_{11} - J_{22}}{\lambda\left(-\lambda^2 + (J_{11} + J_{22})\lambda - J_{11}J_{22} + J_{12}J_{21}\right)} + \frac{1}{\lambda(\lambda - J_{11})}\right)|_{\tau=\tau^*,\lambda=i\omega_0}\right] \\ &= \frac{\omega_0^4 + 2J_{11}^2\omega_0^2 + J_{11}^4 + J_{12}J_{21}(2J_{11}^2 + 2J_{11}J_{22} - J_{12}J_{21})}{(\omega_0^2 + J_{11}^2)\left((J_{11} + J_{22})^2\omega_0^2 + (J_{11}J_{22} - J_{12}J_{21} - \omega_0^2)^2\right)}.\end{aligned} \tag{4.10}$$

Under the condition $2J_{11}^2 + 2J_{11}J_{22} > J_{12}J_{21}$, we have $\mathrm{Re}\left[\left(\frac{d\lambda}{d\tau}\right)^{-1}|_{\tau=\tau^*,\lambda=i\omega_0}\right] > 0$. Hence, the transversal condition is satisfied and the Hopf bifurcation takes place at $\omega = \omega_0$ and $\tau = \tau^*$.

4.2. Stability and direction of Hopf bifurcation

In this subsection, we will deduce the specific formulas that determine the direction, stability, and period of the periodic solutions that emerge from the equilibrium point $E^*(S^*, I^*)$ at the critical values of τ. This will be achieved by applying the normal form and the center manifold theory proposed by Hassard et al. [17] (refer also to [18–20]).

Let $\tilde{S}(x,t) = S(x,\tau t) - S^*$, $\tilde{I}(x,t) = I(x,\tau t) - I^*$. Then, (1.4) (drop the bar) can be expressed as follows:

$$\begin{pmatrix}\dot{S}(t)\\ \dot{I}(t)\end{pmatrix} = \tau M(\tau)\begin{pmatrix}S(t)\\ I(t)\end{pmatrix} + \tau N(\tau)\begin{pmatrix}S(t-1)\\ I(t-1)\end{pmatrix} + \tau F(S,I), \tag{4.11}$$

where

$$\begin{aligned}M(\tau) &= \begin{pmatrix} r\left(1 - \frac{2S^*+I^*}{K}\right) - \frac{\beta I^*}{(1+hS^*)^2} & -\frac{rS^*}{K} - \frac{\beta S^*}{1+hS^*} \\ \frac{\beta I^*}{(1+hS^*)^2} & \frac{\beta S^*}{1+hS^*} - \mu \end{pmatrix}, N(\tau) = \begin{pmatrix}0 & 0\\ 0 & -\rho\end{pmatrix}, \\ F(S,I) &\triangleq \begin{pmatrix}x(S,I)\\ y(S,I)\end{pmatrix} = \begin{pmatrix} \frac{1}{2}x_{20}S^2(t) + x_{11}S(t)I(t) + \frac{1}{2}x_{02}I^2(t) + \frac{1}{6}x_{30}S^3(t) + ... \\ \frac{1}{2}y_{20}S^2(t-1) + y_{11}S(t-1)I(t-1) + \frac{1}{2}y_{02}I^2(t-1) + \frac{1}{6}y_{30}S^3(t-1) + ... \end{pmatrix}\end{aligned}$$

with $x_{ij} = \frac{\partial^{i+j}x(S^*,I^*)}{\partial^i S\partial^j I}$ and $y_{ij} = \frac{\partial^{i+j}y(S^*,I^*)}{\partial^i S\partial^j I}$, $i, j = 1, 2, ...$

Set $\tau = \tau^* + \alpha$. Then, $\alpha = 0$ represents a Hopf bifurcation value for (4.11). For $\phi = (\phi_1, \phi_2)^T \in C\left([-1,0], \mathbb{R}^2\right)$, we define the following:

$$L_\alpha(\phi) = (\tau^* + \alpha)[M(\tau^* + \alpha)\phi(0) + N(\tau^* + \alpha)\phi(-1)]. \tag{4.12}$$

According to the Riesz representation theorem, there exists a 2×2 matrix $\eta(\theta,\alpha)$ with $\theta\in[-1,0]$. The elements of this matrix are functions of a bounded variation, and it holds that

$$L_\alpha(\phi)=\int_{-1}^{0}[d\eta(\theta,\alpha)]\phi(\theta),\quad \phi\in C([-1,0],\mathbb{R}^2). \tag{4.13}$$

Actually, we have the option to choose

$$\eta(\theta,\alpha)=(\tau^*+\alpha)[M(\tau^*+\alpha)\delta(\theta)-N(\tau^*+\alpha)\delta(\theta+1)],$$

i.e.,

$$\eta(\theta,\alpha)=\begin{cases}(\tau^*+\alpha)M(\tau^*+\alpha), & \theta=0,\\ 0, & \theta\in(-1,0),\\ -(\tau^*+\alpha)N(\tau^*+\alpha), & \theta=-1.\end{cases}$$

Additionally, (4.13) is satisfied. Regarding $\phi\in C^1\left([-1,0],\mathbb{R}^2\right)$, we define the operator $A(\alpha)$ in the following way:

$$A(\alpha)\phi(\theta)=\begin{cases}\frac{\mathrm{d}\phi(\theta)}{\mathrm{d}\theta}, & \theta\in[-1,0),\\ \int_{-1}^{0}[\mathrm{d}\eta(\xi,\alpha)]\phi(\xi), & \theta=0.\end{cases}$$

and

$$R(\alpha)\phi(\theta)=\begin{cases}0, & \theta\in[-1,0),\\ h(\alpha,\phi), & \theta=0\end{cases}$$

where

$$h(\alpha,\phi)=(\tau^*+\alpha)\begin{pmatrix}\frac{1}{2}x_{20}S^2(0)+x_{11}S(0)I(0)+\frac{1}{2}x_{02}I^2(0)+\frac{1}{6}x_{30}S^3(0)+...\\ \frac{1}{2}y_{20}S^2(-1)+y_{11}S(-1)I(-1)+\frac{1}{2}y_{02}I^2(-1)+\frac{1}{6}y_{30}S^3(-1)+...\end{pmatrix}.$$

Subsequently, the system (1.4) is tantamount to the operator equation presented as follows: $\dot{u}_t=A(\alpha)u_t+R(\alpha)u_t$, where $u(t)=(S(t),I(t))^T$, and $u_t=u(t+\theta)$, $\theta\in[-1,0]$. For $\psi\in C^1([0,1],(\mathbb{R}^2)^*)$, define the operator

$$A^*\psi(s)=\begin{cases}-\frac{\mathrm{d}\psi(s)}{\mathrm{d}s}, & s\in(0,1],\\ \int_{-1}^{0}\psi(-\xi)\mathrm{d}\eta(\xi,0), & s=0,\end{cases}$$

and a bilinear form $\langle\psi(s),\phi(\theta)\rangle=\overline{\psi}(0)\phi(0)-\int_{-1}^{0}\int_{\xi=0}^{\theta}\overline{\psi}(\xi-\theta)\mathrm{d}\eta(\theta)\phi(\xi)\mathrm{d}\xi$, where $\eta(\theta)=\eta(\theta,0)$. Obviously, A^* and $A(0)$ are adjoint operators. As we have learned from the previous discussion, $\pm i\omega_0\tau^*$ serve as eigenvalues of $A(0)$ and thus are also eigenvalues of A^*. Subsequently, we will compute the eigenvectors. Suppose $q(\theta)$ stands for the eigenvector of matrix $A(0)$ related to the eigenvalue $i\omega_0\tau^*$, and $q^*(s)$ indicates the eigenvector of matrix A^* pertinent to the eigenvalue $-i\omega_0\tau^*$. Then, it follows that $A(0)q(\theta)=i\omega_0\tau^*q(\theta)$ and $A^*q^*(s)=-i\omega_0\tau^*q(s)$. Through simple calculations, we may acquire that $q(\theta)=(q_1,q_2)^Te^{i\omega_0\tau^*\theta}$, $\theta\in[-1,0]$, and $q^*(s)=(1/\overline{D})(q_1^*,q_2^*)^Te^{i\omega_0\tau^*s}$, $s\in[0,1]$, where $q_1=q_1^*=1$, $q_2=\frac{r\left(1-\frac{2S^*+I^*}{K}\right)-\frac{\beta I^*}{(1+hS^*)^2}-\mu-i\omega_0}{\frac{rS^*}{K}+\frac{\beta}{1+hS^*}}$, and $q_2^*=\frac{r\left(\frac{2S^*+I^*}{K}-1\right)+\frac{\beta I^*}{(1+hS^*)^2}+\mu-i\omega_0}{\frac{\beta I^*}{(1+hS^*)^2}}$. Let $D=1+\overline{q_2^*}q_2\left(1-\rho\tau^*e^{-i\omega_0\tau^*}\right)$; then, $\langle q^*(s),q(\theta)\rangle=1$ and $\langle q^*(s),\overline{q}(\theta)\rangle=0$.

Adopting the same algorithms and a comparable computation process to that of Hassard et al. [17], we derive the coefficients which determine the significant quantities as follows:

$$
\begin{aligned}
g_{20} =& \frac{\tau^*}{D}[\overline{q^*}_1(x_{20}q_1^2 + 2x_{11}q_1q_2 + x_{02}q_2^2) + \overline{q^*}_2(y_{20}q_1^2 + 2y_{11}q_1q_2 + y_{02}q_2^2)],\\
g_{11} =& \frac{\tau^*}{D}[\overline{q^*}_1(x_{20}|q_1|^2 + x_{11}(q_1\overline{q}_2 + \overline{q}_1q_2) + x_{02}|q_2|^2) + \overline{q^*}_2(y_{20}|q_1|^2 + y_{11}(q_1\overline{q}_2 + \overline{q}_1q_2) + y_{02}|q_2|^2)],\\
g_{02} =& \frac{\tau^*}{D}[\overline{q^*}_1(x_{20}\overline{q}_1^2 + 2x_{11}\overline{q}_1\overline{q}_2 + x_{02}\overline{q}_2^2) + \overline{q^*}_2(y_{20}\overline{q}_1^2 + 2y_{11}\overline{q}_1\overline{q}_2 + y_{02}\overline{q}_2^2)],\\
g_{21} =& \frac{\tau^*}{D}\{\overline{q^*}_1[x_{20}(W_{20}^{(1)}(0)\overline{q}_1 + 2W_{11}^{(1)}(0)q_1) + x_{11}(W_{20}^{(1)}(0)\overline{q}_2 + 2W_{11}^{(1)}(0)q_2 + 2W_{11}^{(2)}(0)q_1 + W_{20}^{(2)}(0)\overline{q}_1) +\\
& x_{02}(W_{20}^{(2)}(0)\overline{q}_2 + 2W_{11}^{(2)}(0)q_2) + x_{30}q_1^2\overline{q}_1 + x_{21}(q_1^2\overline{q}_2 + 2|q_1|^2q_2) + x_{12}(q_2^2\overline{q}_1 + 2|q_2|^2q_1) + x_{03}q_2^2\overline{q}_2] +\\
& \overline{q^*}_2[y_{20}(W_{20}^{(1)}(0)\overline{q}_1 + 2W_{11}^{(1)}(0)q_1) + y_{11}(W_{20}^{(1)}(0)\overline{q}_2 + 2W_{11}^{(1)}(0)q_2 + 2W_{11}^{(2)}(0)q_1 + W_{20}^{(2)}(0)\overline{q}_1) +\\
& y_{02}(W_{20}^{(2)}(0)\overline{q}_2 + 2W_{11}^{(2)}(0)q_2) + y_{30}q_1^2\overline{q}_1 + y_{21}(q_1^2\overline{q}_2 + 2|q_1|^2q_2) + y_{12}(q_2^2\overline{q}_1 + 2|q_2|^2q_1) + y_{03}q_2^2\overline{q}_2]\},
\end{aligned}
$$

where

$$
\begin{aligned}
W_{20}(\theta) &= \frac{\mathrm{i}g_{20}}{\omega_0\tau^*}q(\theta) + \frac{\mathrm{i}\overline{g}_{02}}{3\omega_0\tau^*}\overline{q}(\theta) + B_1e^{2\mathrm{i}\omega_0\tau^*\theta},\\
W_{11}(\theta) &= -\frac{\mathrm{i}g_{11}}{\omega_0\tau^*}q(\theta) + \frac{\mathrm{i}\overline{g}_{11}}{\omega_0\tau^*}\overline{q}(\theta) + B_2,
\end{aligned}
$$

with

$$
B_1 = \begin{pmatrix} 2i\omega_0 - r\left(1 - \frac{2S^*+I^*}{K}\right) + \frac{\beta I^*}{(1+hS^*)^2} + \mu & \frac{rS^*}{K} + \frac{\beta}{1+hS^*} \\ -\frac{\beta I^*}{(1+hS^*)^2} & 2i\omega_0 - \frac{\beta S^*}{1+hS^*} + \mu + \rho e^{-2i\omega_0\tau} \end{pmatrix}^{-1} \times \begin{pmatrix} \frac{1}{2}x_{20}q_1^2 + x_{11}q_1q_2 + \frac{1}{2}x_{02}q_2^2 \\ \frac{1}{2}y_{20}q_1^2 + y_{11}q_1q_2 + \frac{1}{2}y_{02}q_2^2 \end{pmatrix},
$$

$$
B_2 = \begin{pmatrix} r\left(\frac{2S^*+I^*}{K} - 1\right) + \frac{\beta I^*}{(1+hS^*)^2} + \mu & \frac{rS^*}{K} + \frac{\beta}{1+hS^*} \\ -\frac{\beta I^*}{(1+hS^*)^2} & -\frac{\beta S^*}{1+hS^*} + \mu + \rho \end{pmatrix}^{-1} \times \begin{pmatrix} \frac{1}{2}x_{20}|q_1|^2 + x_{11}(q_1\overline{q_2} + \overline{q_1}q_2) + \frac{1}{2}x_{02}|q_2|^2 \\ \frac{1}{2}y_{20}|q_1|^2 + y_{11}(q_1\overline{q_2} + \overline{q_1}q_2) + \frac{1}{2}y_{02}|q_2|^2 \end{pmatrix}.
$$

Consequently, we can compute the following values:

$$
\begin{aligned}
c_1(0) &= \frac{i}{2\omega_0\tau^*}\left(g_{11}g_{20} - 2|g_{11}|^2 - \frac{1}{3}|g_{02}|^2\right) + \frac{1}{2}g_{21},\\
\mu_2 &= -\frac{\mathrm{Re}(c_1(0))}{\mathrm{Re}(\lambda'(\tau^*))},\\
\beta_2 &= 2\,\mathrm{Re}(c_1(0)),\\
T_2 &= -\frac{\mathrm{Im}(c_1(0)) + \mu_2\mathrm{Im}(\lambda'(\tau^*))}{\omega_0\tau^*}.
\end{aligned}
$$

Meanwhile, we can establish the following theorem.

Theorem 4.1. *With regard to any critical value τ^*, the following outcomes are obtained:*

(i) When $\mu_2 > 0$, the Hopf bifurcation is of a forward type; whereas if $\mu_2 < 0$, then it is of a backward type.

(ii) When $\beta_2 > 0$, the bifurcating periodic solutions on the center manifold exhibit orbital asymptotic instability; conversely, when $\beta_2 < 0$, such solutions display orbital asymptotic stability.

(iii) When $T_2 > 0$, the period increases; when $T_2 < 0$, the period decreases.

5. Numerical simulations

The following presents specific examples using the MATLAB tool to verify the results of the above theoretical analysis. With data given by [1], we investigate the impact of the delayed death of infected individuals on the dynamics. In addition, we set a recapitulation of model parameters and their estimation means (Table 1).

Table 1. A recapitulation of model parameters and their estimation means.

Parameter	Meaning	Unit	Evaluation and associated causal impact
r	regeneration rate	yr^{-1}	0.712. Estimated based on the data in [22] from 1975.
K	carrying capacity	/	120. Calculated based on the data in [1].
β	transmission rate per capita	$(yr^{-1})^{-1}$	0.0174. Rectified with reference to disease records in 2018 [1].
h	saturated incidence rate	yr^{-1}	0.005. Calculated based on the data in [1].
μ	natural mortality rate	yr^{-1}	0.05. Derived with reference to [22].
ρ	disease-induced mortality rate	yr^{-1}	0.0877. Derived based on the average annual mortality rate (AMR) within the period of 2021–2022 in Wytham Woods [1].

Equation system (1.4) possesses the sole positive equilibrium point $E^*(8.1911, 27.1063)$. Moreover, it can be readily determined that $\tau_0 = 3.7128$.

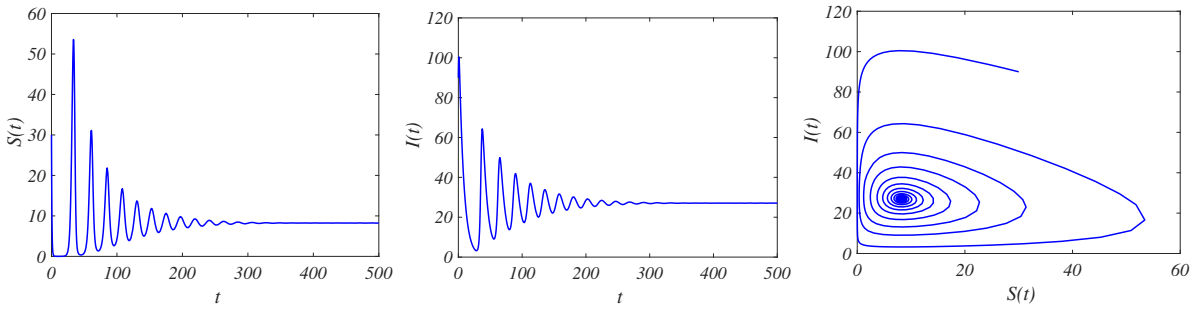

Figure 1. The changes over time of the susceptible $S(t)$ and infective $I(t)$ when $\tau = 0$. And the initial value is (30, 90).

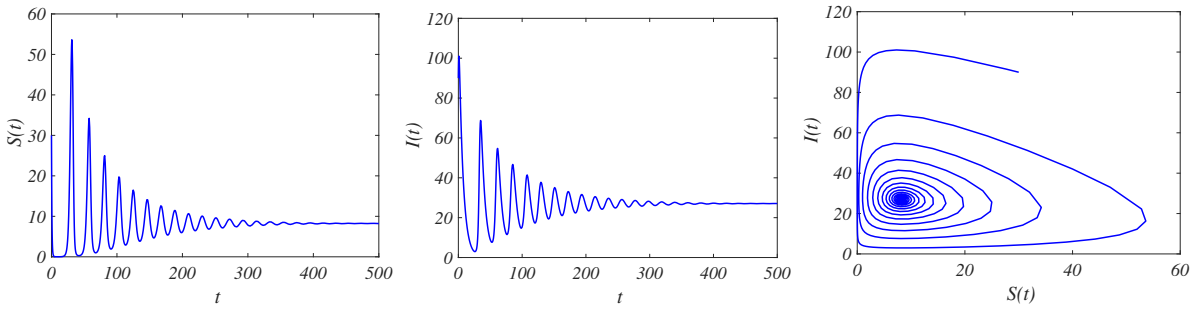

Figure 2. Temporal behavior of the susceptible individuals $S(t)$, infective individuals $I(t)$ with $\tau = 1.25$. And the initial value is (30, 90).

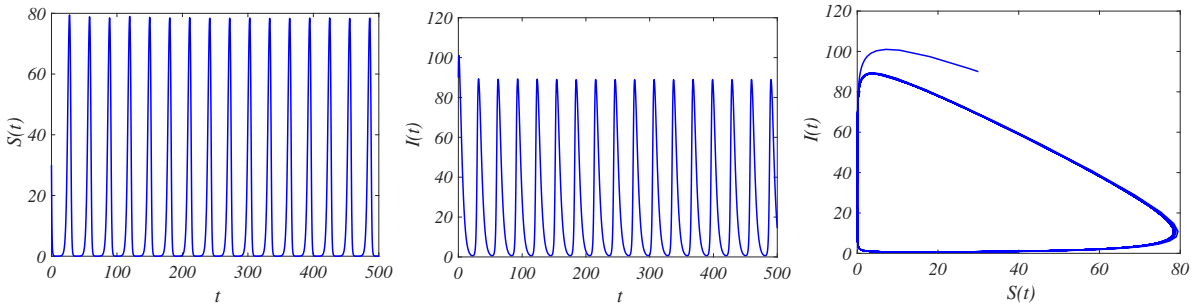

Figure 3. Temporal behavior of the susceptible, infective individuals $S(t), I(t)$ with $\tau = 3.72$. And the initial value is (30, 90).

For the case when $\tau = 0$, it is observable from Figure 1 that E^* exhibits asymptotic stability. As illustrated in Figure 2, the equilibrium E^* of system (1.4) exhibits asymptotic stability when $\tau_0 > \tau = 1.25$. Moreover, as depicted in Figure 3, upon τ traversing the critical value τ_0, the stability of E^* is lost and a set of periodic solutions bifurcating from E^* emerges.

Biologically, the initial values correspond to the initial densities of susceptible and infected trees in the corresponding region. As the epidemic evolves, the population densities of susceptible and infected trees undergo corresponding changes. From Figures 1-3, it can be observed that when the time delay of the infected trees' death is relatively small, the densities of the two populations eventually reach a stable state. When the time delay of the infected trees' death is relatively large, the epidemic exhibits periodic fluctuations. In particular, the periodic fluctuations of the infectious disease are relatively large under this set of parameters, and small perturbations may lead to the extinction of either the susceptible population or the infected population.

The model was verified with data from areas that possess an extensive disease history and prolonged tree mortality records. Three regions were selected, namely Latvia [22], Norway [23], and Switzerland [24], which correspond to Figures (A), (B), and (C), respectively. The horizontal axis stands for the number of years passed since the occurrence of ash dieback at the site, while the vertical axis denotes the cumulative mortality rate (CMR, %). The blue curve represents the predicted values of the model, and the red curve represents the observed values. The performance of the model was judged by observing the trends and fitting degrees of the red and blue curves.

As can be seen from Figure 4, the trends of the observed curve and the predicted curve are approximately the same. In the Latvia site, the predicted value shows a slower growth the in cumulative mortality rate 10 years after the exposure to the disease, and the change in the observed cumulative mortality rate tends to flatten after the 20th year. In the Norway site, around the 7th year after the exposure to the disease, the predicted value shows different forms of change. Before the 7th year, the predicted value shows a faster cumulative mortality rate, and after the 7th year, it shows a slower cumulative mortality rate. For the observed value, the growth rate of the cumulative mortality rate is relatively fast from the 4th to the 8th year after the exposure to the disease, and then slows down after the 8th year. In the Switzerland site, before the 9th year after the exposure to the disease, the predicted value shows a faster growth in the cumulative mortality rate. For the observed value, the cumulative mortality rate shows a relatively fast growth rate after the sixth year of exposure to the disease. There are discrepancies between the predicted values and model values in certain years, which may be due to potential regional differences in disease progression or environmental factors

across various regions. However, the predicted values reflect the development trend of the cumulative mortality rate to a certain extent. Overall, this model captures the mortality dynamics in these three regions and effectively validates the model.

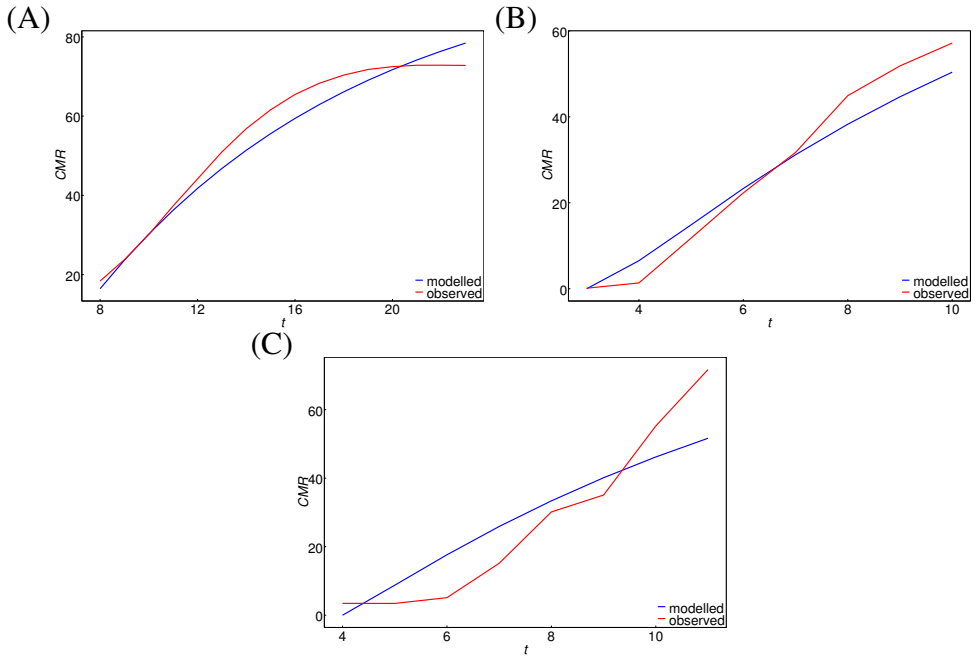

Figure 4. Model verification employing data from areas with an extended disease background and prolonged tree mortality logs.

6. Sensitivity analysis

Sensitivity analysis is crucial to understand the population behavior in an ecosystem and identify the key parameters. Using this, the relative impact of model parameters on the system can be evaluated. First, the initial values of each parameter are set as follows:

$$r = 0.712, \quad K = 120, \quad \beta = 0.0174, \quad \mu = 0.05, \quad \rho = 0.0877.$$

Then, the values of the remaining parameters as appropriate. At present, the aim is to figure out which parameters play a significant role in bringing about variability in the behavior of the positive equilibrium state. By following the procedure detailed in Chitnis et al. [21], it is possible to calculate the sensitivity indices associated with the model parameters. For this, the dependent factors (S, I) are substituted with (u_1, u_2), and the system parameters $(r, K, \beta, h, \mu, \rho)$ by $(U_1, U_2, U_3, U_4, U_5, U_6)$, the equilibrium point E^* by (u_1^*, u_2^*). Afterward, the equilibrium equations may be presented in the following manner:

$$\begin{cases} f_i(u_1, u_2, U_1, U_2, U_3, U_4, U_5, U_6) = 0, \quad i = 1, 2, \\ f_1(u_1, u_2, U_1, U_2, U_3, U_4, U_5, U_6) = U_1 u_1 \left(1 - \dfrac{u_1 + u_2}{U_2}\right) - \dfrac{U_3 u_1 u_2}{1 + U_4 u_1} - U_5 u_1, \\ f_2(u_1, u_2, U_1, U_2, U_3, U_4, U_5, U_6) = \dfrac{U_3 u_1 u_2}{1 + U_4 u_1} - U_5 u_2 - U_6 u_2. \end{cases} \tag{6.1}$$

Let $AX_j = Y_j$, where $A = \begin{bmatrix} a_{11} & a_{12} \\ a_{21} & a_{22} \end{bmatrix}, X_j = \begin{bmatrix} \frac{\partial u_1^*}{\partial U_j} \\ \frac{\partial u_2^*}{\partial U_j} \end{bmatrix}, K_j = \begin{bmatrix} \frac{\partial f_1}{\partial U_j} \\ \frac{\partial f_2}{\partial U_j} \end{bmatrix}$, $a_{11} = -U_5 - \frac{U_1 u_1}{U_2} + \frac{U_3 U_4 u_1 u_2}{(1+U_4 u_1)^2} - \frac{U_3 u_2}{1+U_4 u_1} + U_1\left(1 - \frac{u_1+u_2}{U_2}\right), a_{12} = -\frac{U_1 u_1}{U_2} - \frac{U_3 u_1}{1+U_4 u_1}, a_{21} = -\frac{U_3 U_4 u_1 u_2}{(1+U_4 u_1)^2} + \frac{U_3 u_2}{1+U_4 u_1}$, and $a_{22} = -U_5 - U_6 + \frac{U_3 u_1}{1+U_4 u_1}$. Finally, the sensitivity index of the equilibrium point E^*, u_i^*, to the parameter, U_j, is given by $\frac{\partial u_i^*}{\partial U_j}\frac{U_j}{u_i^*}$, $1 \le i \le 2$, $1 \le j \le 6$. The sensitivity factors of the model variables are relevant to the positive equilibrium, which is acquired in this way, are shown in Table 2. According to Table 2, it can be easily determined that for the component S^*, the most sensitive parameter is β, followed by μ, h, ρ, r, and K. Likewise, it is observed that for the other component I^*, the system parameter μ is also the most sensitive one, trailed by r, K, β, ρ and h.

Table 2. Sensitivity coefficients of the model (1.4)'s system parameters with respect to the equilibrium point E^*.

Parameter	S^*	I^*
r	-6.42484×10^{-6}	-7.022110
K	-4.56194×10^{-7}	-0.498602
β	1.26578	-0.270817
h	-0.265776	0.0568638
μ	-1.11385	7.86228
ρ	-0.151921	0.145994

Furthermore, as shown in Figure 5, the manner in which the peak value of the infected population varies with the alteration of a specific system parameter can be discerned.

By observing Figure 5, we find that the contact rate (β), the natural mortality rate of the species (μ), and the saturated incidence rate (h) are three important parameters of the system model (1.4). Therefore, in the subsequent research, we will focus on estimating the impacts of these three parameters on the current dynamics of the model (1.4).

From Figure 6(A),(B), when the value of the transmission rate (β) increases from 0.015 to 0.02, the equilibrium point of the susceptible population shows a decreasing trend. In contrast, the two figures indicate that the equilibrium point of the infected population is monotonically increasing with respect to the transmission rate (β), that is, as the value of the transmission rate (β) increases, the populations of the infected population rises. This trend is further illustrated in Figure 6(C),(D), which show the variation of the quantities of $S(t)$ and $I(t)$ when β takes different values within the interval $[0.015, 0.020]$. Apparently, when β changes within this range, the quantity of susceptible individuals declines and that of the infected individuals rises, which is in line with what is shown in Figure 6(A),(B).

Similarly, one can evaluate the impact of the natural mortality rate (μ) on the quantities of the susceptible and infected populations through Figure 7(A),(B). From these figures, as the value of the system parameter μ increases from 0.04 to 0.06, the curve of the susceptible population shows an upward trend. However, the opposite characteristic has been recorded for the infected population. This pattern is more clearly demonstrated in Figure 7(C),(D), which depict the effect of the quantities of $S(t)$ and $I(t)$ when μ takes different values within the interval $[0.04, 0.06]$. It is evident that as μ varies within this range, the number of susceptible individuals increases while the number of infected

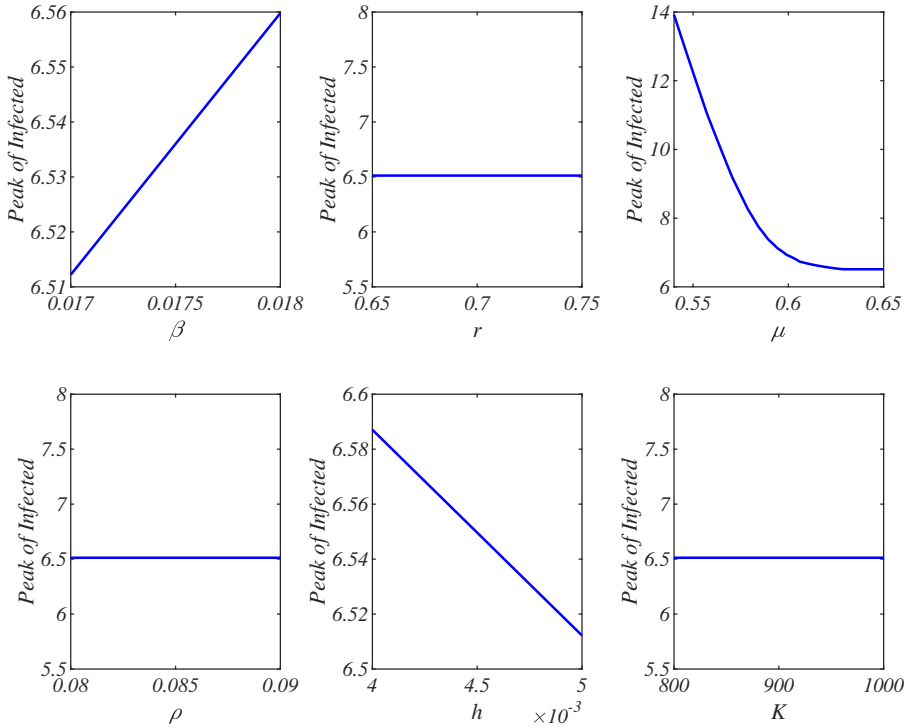

Figure 5. The peak value of the infected population changes with the variation of a certain system parameter.

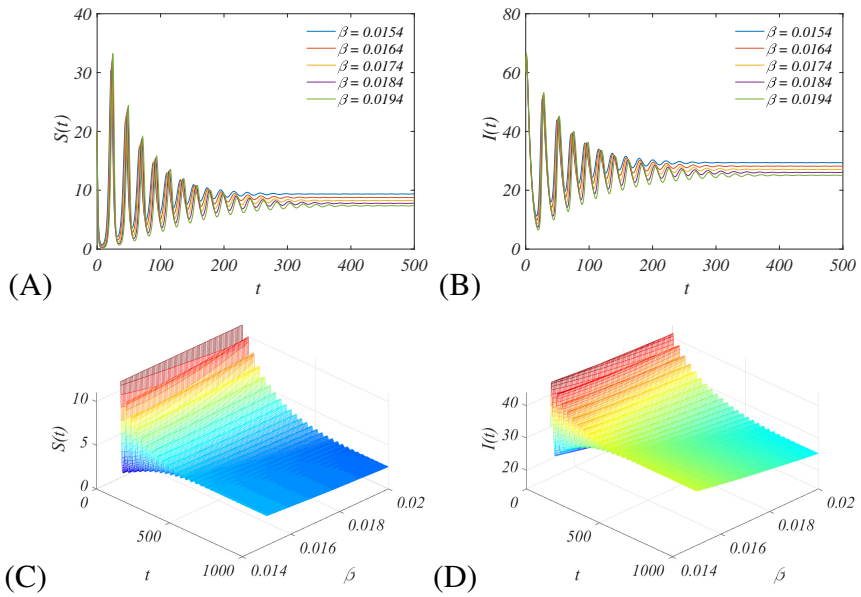

Figure 6. (A) and (B) are the variation of the number of $S(t)$ and $I(t)$ when β takes different values of $0.0154, 0.0164, 0.0174, 0.0184, 0.0194$, respectively. (C) and (D) are the variation of the quantities of $S(t)$ and $I(t)$ when β takes different values within the interval $[0.015, 0.020]$, respectively.

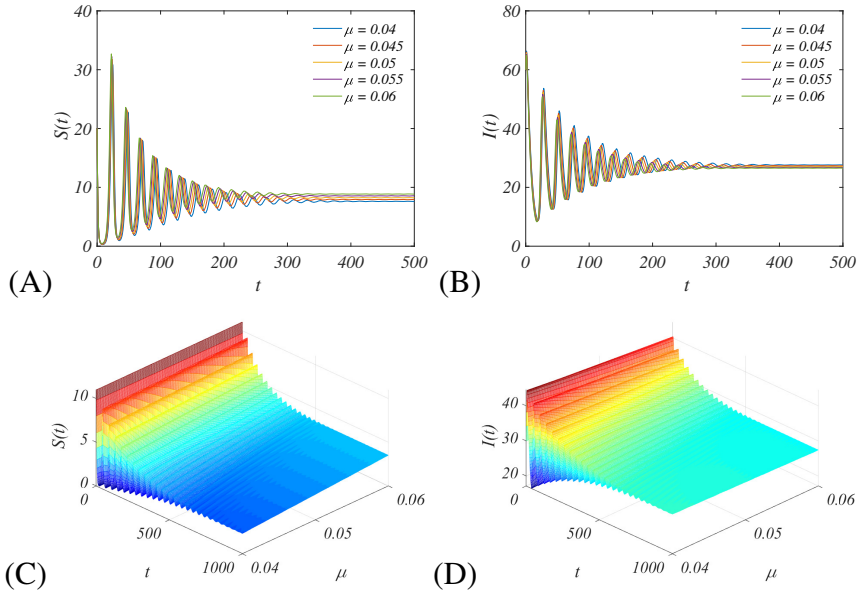

Figure 7. (A) and (B) are the effect of the number of $S(t)$ and $I(t)$ when μ takes different values of $0.04, 0.045, 0.05, 0.055, 0.06$, respectively. (C) and (D) are the effect of the quantities of $S(t)$ and $I(t)$ when μ takes different values within the interval $[0.04, 0.06]$, respectively.

individuals decreases, which is in line with the observations in Figure 7(A),(B).

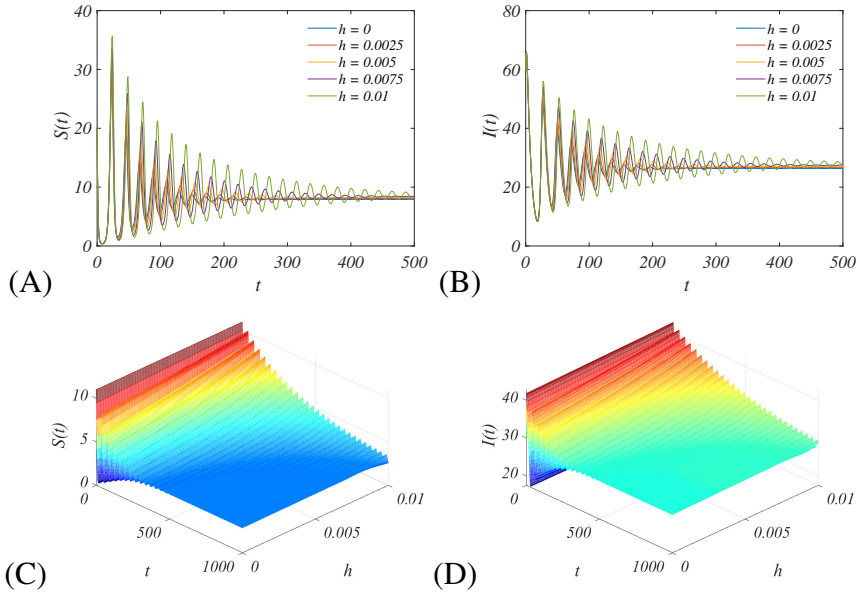

Figure 8. (A) and (B) are the influence of the number of $S(t)$ and $I(t)$ when h takes different values of $0, 0.0025, 0.005, 0.0075, 0.01$, respectively. (C) and (D) are the influence of the quantities of $S(t)$ and $I(t)$ when h takes different values within the interval $[0, 0.01]$, respectively.

Figure 8(A),(B) exhibit the changes in the population quantities with varying values of the saturated incidence rate (h). It can be clearly seen that as the saturated incidence rate (h) increases, both the quantity of the susceptible population and the quantity of the infected population rise. Moreover, with an increase in h, the speed at which the system reaches a stable state gradually slows down. This phenomenon is further illustrated in Figure 8(C),(D), which show the influence of the quantities of $S(t)$ and $I(t)$ when h takes different values within the interval $[0, 0.01]$. As can be observed, as h varies within this interval, both the number of susceptible individuals and the number of infected individuals increase, and the rate of stabilization decreases, which is consistent with the trends depicted in Figure 8(A),(B).

A sensitivity analysis has a strong practical significance. For example, in biology, an increase in the natural mortality rate is beneficial to susceptible populations and has a negative impact on the infected populations. The rise in natural mortality rate prioritizes the elimination of susceptible populations with poor disease resistance, thus leaving the remaining ones with a stronger overall disease resistance. However, this imposes negative effects on infected populations: the increase in natural mortality rate directly raises their survival risk, and may further reduce their survival probability due to the pathogen spread and insufficient prevention and control resources.

7. Discussion and conclusions

This paper centered on an infectious disease model that incorporated a delayed mortality rate and the Holling-II functional response function.

7.1. Bifurcation analysis without time delay

Primarily, the research revealed the presence of a transcritical bifurcation at the equilibrium point E_1. When the delayed mortality rate ρ changes, the stability of the equilibrium point alternates and the dynamic behavior of the system significantly changes. When ρ nears the critical value, a shift in the stability from one unstable state to another transpires, which is of a crucial significance to comprehend the dynamic alterations in disease transmission. In the vicinity of the equilibrium point E^*, the direction and stability of the Hopf bifurcation are ascertained based on the sign of the first Lyapunov number $\mathcal{L}_1$. When $\mathcal{L}_1 > 0$, a supercritical Hopf bifurcation occurs. Subsequent to the bifurcation, the system exhibits stable periodic oscillations, with the disease transmission and population quantity periodically varying and stably around the positive equilibrium. Conversely, when $\mathcal{L}_1 < 0$, a subcritical Hopf bifurcation takes place. Even though there are periodic oscillations, they are unstable. A small external disturbance can make the system move away from the limit cycle, which makes the changes in disease transmission and population quantity complicated and hard to predict.

7.2. Discussion of numerical simulation

In the numerical simulation section, through the observation and analysis of Figures 1-3, we can obtain the dynamic behaviors of the infectious disease model under different delay times. These results are of great significance for the in-depth understanding of the model characteristics, thereby predicting the trend of disease transmission, and formulating relevant strategies.

From Figure 1, when $\tau = 0$, the changes of the number of susceptible individuals $S(t)$ and the number of infected individuals $I(t)$ in the system over time exhibit a certain pattern. In the initial stage,

the values of $S(t)$ and $I(t)$ fluctuate with time; however, as time goes by, they gradually approach a stable value. This indicates that in the absence of the influence of delayed mortality, the system can reach a stable state relatively quickly, and this stable state can be maintained for a long time. This result is consistent with the conclusion about the stability of the system equilibrium point in the case of no delay in the theoretical analysis, thus further verifying that the system has good stability when there is no delay, that is, the dynamic behavior of the system is relatively simple and predictable under the condition of no delay.

In Figure 2, when the time delay $\tau = 1.25$, the curves of $S(t)$ and $I(t)$ show that the system still maintains a certain stability. Although the value of τ is not zero, at this time, the system does not show an obvious instability due to the delay factor. The number of susceptible individuals $S(t)$ fluctuates within a relatively stable range, and the number of infected individuals $I(t)$ shows a similar stable fluctuation trend. This indicates that under this delay time, the stability of the system is still relatively strong, the delayed death factor has not yet had a significant interference on the dynamic behavior of the system, and the system can still be maintained in a relatively stable state; however, compared with when $\tau = 0$, the dynamic changes of the system become slightly more complex.

From Figure 3, when τ increases to 3.72 (exceeding the critical value τ_0), the behavior of the system significantly changes. At this time, the number of susceptible individuals $S(t)$ and the number of infected individuals $I(t)$ no longer show a stable trend, but begin to exhibit periodic oscillations. These periodic oscillations indicate that the system have entered a Hopf bifurcation state, which is consistent with the conditions and results of the Hopf bifurcation in the theoretical analysis. At this time, the disease transmission and population quantity begin to periodically change around the equilibrium point, and the dynamic behavior of the system becomes more complex. Moreover, this periodic change will continue to exist, which has an important impact on the spread of the disease and the population dynamics, and further in-depth research is needed to understand and predict the behavior of the system in this state.

Overall, with the change of the delay time τ, the dynamic behavior of the system has changed from stable to periodic oscillations. When $\tau = 0$ and τ is less than the critical value, the system shows a stable state, while when τ exceeds the critical value (such as $\tau = 3.72$), the system exhibits periodic oscillations. These results fully verify the conclusions about the stability of the equilibrium point and the existence of Hopf bifurcation in the theoretical analysis. Through numerical simulation, it intuitively shows the important influence of the delayed death factor on the dynamic behavior of the infectious disease model, thus providing a powerful basis to further study the disease transmission mechanism and formulate the corresponding prevention and control strategies.

Next, through the comparative analysis of the observed and predicted values in the three regions of Latvia, Norway, and Switzerland, we verified the effectiveness of the model in describing the spread and lethality of ash dieback, and at the same time, revealed the regional differences and dynamic change laws of the disease spread. By comparing the trends of the observed and predicted values and the growth rate of the cumulative mortality rate, the dynamic characteristics of ash dieback in different regions were analyzed in depth. For example, in the Latvia site, 10 years after the disease exposure, the predicted value showed a slower growth in the cumulative mortality rate, and the observed value was stable after the 20th year, thus indicating that the disease spread in this region was relatively slow. In the Norway site, the predicted value showed a faster cumulative mortality rate, and after the 7th year, it showed a slower cumulative mortality rate, while the observed value grew relatively fast from

the 4th to the 8th year and then was stable after the 8th year, thus reflecting the high variability of the disease spread in the early and middle stages in Norway. In the Switzerland site, the predicted value showed a faster growth in the cumulative mortality rate, and the observed value showed a relatively fast growth rate after the 6th year, thus indicating that the disease spread in this region may be affected by special environmental or management measures. This study not only provides a scientific tool for the prevention and control of ash dieback, but also provides practical experience for the development and optimization of ecological models, and has an important reference significance for the research of similar ecosystem diseases.

7.3. Discussion of sensitivity analysis

In the sensitivity analysis section, the study explored the impact of changing the system parameter values on the model dynamics. From the results, it can be seen that each parameter has a significant and different influence on the model dynamics, and these findings are of a great significance for in-depth understanding of the model characteristics and formulating targeted strategies.

First, we analyzed the sensitivity indices of each parameter. From the results, we found that for the component S^* of the coexistence equilibrium point, the most sensitive parameter is β. This indicates that the change of β has the greatest impact on the number of susceptible populations. For example, when studying disease transmission control measures, it is necessary to focus on β related factors, such as intervention in the transmission routes. For I^*, the most sensitive parameter is μ. This shows that the natural mortality rate μ has a significant impact on the number of infected populations, and its effect on the number of infected individuals should be considered when formulating disease prevention and control strategies.

Second, we selected three important parameters and discussed the impact of parameter changes on the population quantity. From Figure 6, it can be seen that within the interval $[0.015, 0.020]$, an increase in β led to a decrease in the number of susceptible individuals and an increase in the number of infected individuals. This indicates that β is positively correlated with disease transmission. When preventing and controlling, the influence of β related factors can be reduced, such as strengthening the protective measures to reduce the probability of contact transmission. As shown in Figure 7, within the interval $[0.04, 0.06]$, an increase in μ causes the number of susceptible individuals to increase and the number of infected individuals to decrease. This shows that μ has an inhibitory effect on the infected population. In ecosystem management, μ can be adjusted by controlling the environmental factors. Figure 8 shows that within the interval $[0, 0.01]$, the change in h made the numbers of both increase and the stabilization speed decrease. This means that h affects the disease transmission speed and system stability. In the application of the model, the impact of h on the population quantity and stability needs to be comprehensively considered.

In summary, the sensitivity analysis provides an important basis to understand the model dynamics and help to formulate more effective strategies in disease prevention and control and ecosystem management. However, the existing methods inevitably have uncertainties. Therefore, researchers can explore more advanced parameter estimation techniques, such as combining machine learning algorithms with field monitoring data, to improve the accuracy of parameter estimation. These will be incorporated into future work.

Use of AI tools declaration

The authors declare they have not used Artificial Intelligence (AI) tools in the creation of this article.

Acknowledgments

This research is supported by Heilongjiang Provincial Natural Science Foundation (PL2024A002).

Conflict of interest

The authors declare there is no conflicts of interest.

References

1. H. Wu, C. A. L. Dahlsjo, Y. Malhi, Evaluating the impact of an invasive pathogen on tree population decline: An evidence based modelling approach, *For. Ecol. Manage.*, **566** (2024), 122098. https://doi.org/10.1016/j.foreco.2024.122098
2. K. Mokni, M. Ch-Chaoui, B. Mondal, U. Ghosh, Rich dynamics of a discrete two dimensional predator-prey modelusing the NSFD scheme, *Math. Comput. Simul.*, **225** (2024), 992–1018. https://doi.org/10.1016/j.matcom.2023.09.024
3. M. Ch-Chaoui, K. Mokni, A multi-parameter bifurcation analysis of a prey-predator model incorporating the prey Allee effect and predator-induced fear, *Nonlinear Dyn.*, **113** (2025), 18879–18911. https://doi.org/10.1007/s11071-025-11063-w
4. K. Mokni, H. Mouhsine, M. Ch-Chaoui, Multi-parameter bifurcations in a discrete Ricker-type predator-prey model with prey immigration, *Math. Comput. Simul.*, **233** (2025), 39–59. https://doi.org/10.1016/j.matcom.2025.01.020
5. H. Mouhsine, K. Mokni, M. Ch-Chaoui, Exploring multi-parameter bifurcations and immigrationdriven dynamics in a discrete-time Bazykin-Berezovskaya prey-predator model, *Nonlinear Dyn.*, **113** (2025), 34101–34131. https://doi.org/10.1007/s11071-025-11818-5
6. G. Charron, M. Gauthier, V. Aucoin, P. Tanguay, Outbreak of Phytophthora abietivora in a Québec forest nursery: Emergence of a new Phytophthora tree pathogen?, *For. Pathol.*, **55** (2025), e70041. https://doi.org/10.1111/efp.70041
7. H. W. Hethcote, The mathematics of infectious diseases, *SIAM Rev.*, **42** (2000), 599–653. https://doi.org/10.1137/S0036144500371907
8. L. Chen, J. Sun, Global stability of an SI epidemic model with feedback controls, *App. Math. Lett.*, **28** (2014), 53–55. https://doi.org/10.1016/j.aml.2013.09.009
9. L. Wang, D. Zhou, Z. Liu, D. Xu, X. Zhang, Media alert in an SIS epidemic model with logistic growth, *J. Biol. Dyn.*, **11** (2016), 120–137. https://doi.org/10.1080/17513758.2016.1181212
10. R. M. Anderson, R. M. May, Population biology of infectious diseases, *Nature*, **280** (1979), 361–367. https://doi.org/10.1038/280361a0

11. S. Gao, L. Chen, J. J. Nieto, A. Torres, Analysis of a delayed epidemic model with pulse vaccination and saturation incidence, *Vaccine*, **24** (2006), 6037–6045. https://doi.org/10.1016/j.vaccine.2006.05.018
12. T. Zhang, Z. Teng, Pulse vaccination delayed SEIRS epidemic model with saturation incidence, *Appl. Math. Modell.*, **32** (2008), 1403–1416. https://doi.org/10.1016/j.apm.2007.06.005
13. D. Xiao, S. Ruan, Global analysis in a predator-prey system with nonmonotonic functional response, *SIAM J. Appl. Math.*, **61** (2001), 1445–1472. https://doi.org/10.1137/S0036139999361896
14. F. Brauer, C. Castillo-Chavez, *Mathematical Models in Population Biology and Epidemiology*, Springer, New York, 2012. https://doi.org/10.1007/978-1-4614-1686-9
15. M. Kot, *Elements of Mathematical Ecology*, Cambridge University Press, Cambridge, 2001. https://doi.org/10.1017/CBO9780511608520
16. B. Pirayesh, A. Pazirandeh, M. Akbari, Local bifurcation analysis in nuclear reactor dynamics by Sotomayor's theorem, *Ann. Nucl. Energy*, **94** (2016), 716–731. https://doi.org/10.1016/j.anucene.2016.04.021
17. B. Hassard, N. Kazarinoff, Y. Wan, *Theory and Applications of Hopf Bifurcation*, Cambridge University Press, Cambridge, 1981.
18. J. Wei, S. Ruan, Stability and bifurcation in a neural network model with two delays, *Phys. D*, **130** (1999), 255–272. https://doi.org/10.1016/S0167-2789(99)00009-3
19. J. Wei, M.Y. Li, Hopf bifurcation analysis in a delayed Nicholson blowflies equation, *Nonlinear Anal.*, **60** (2005), 1351–1367. https://doi.org/10.1016/j.na.2003.04.002
20. Y. Qu, J. Wei, Bifurcation analysis in a predator-prey system with stage-structure and harvesting, *J. Franklin Inst.*, **347** (2010), 1097–1113. https://doi.org/10.1016/j.jfranklin.2010.03.017
21. N. Chitnis, J. M. Hyman, J. M. Cushing, Determining important parameters in the spread of malaria through the sensitivity analysis of a mathematical model, *Bull. Math. Biol.*, **70** (2008), 1272–1296. https://doi.org/10.1007/s11538-008-9299-0
22. I. Matisone, R. Matisons, A. Jansons, The Struggle of Ash-Insights from long-term survey in Latvia, *Forests*, **12** (2021), 340. https://doi.org/10.3390/f12030340
23. V. Timmermann, N. E. Nagy, A. M. Hietala, I. Borja, H. Solheim, Progression of ash dieback in Norway related to tree age, disease history and regional aspects, *Balt. For*, **23** (2017), 150–158.
24. S. Klesse, G. von Arx, M. M. Gossner, C. Hug, A. Rigling, V. Queloz, Amplifying feedback loop between growth and wood anatomical characteristics of Fraxinus excelsior explains size-related susceptibility to ash dieback, *Tree Physiol.*, **41** (2021), 683–696. https://doi.org/10.1093/treephys/tpaa091

AIMS Press